

Inertia in skyrmions confined to one-dimensional geometries

Koichiro Takahashi,^{1,*} Sergey S. Pershoguba,^{1,†} and Jiadong Zang^{1,2,‡}

¹*Department of Physics and Astronomy, University of New Hampshire, Durham, New Hampshire 03824, USA*

²*Materials Science Program, University of New Hampshire, Durham, New Hampshire 03824, USA*

(Dated: September 27, 2024)

Magnetic skyrmions are conventionally attributed to having zero mass. In contrast, we show that skyrmions confined to one-dimensional geometries generically acquire mass (inertia) due to the combined effects of the skyrmion Hall effect and the elasticity of the system. We investigate the massive behavior of the skyrmion for a simplified periodic model of the disorder. We show that skyrmion mass lowers the critical depinning force and leads to a step-like behavior in the skyrmion velocity-vs-current curves, which were recently observed in experiments. Finite mass could also lead to hysteresis in the velocity-vs-current curves.

I. INTRODUCTION

Magnetic skyrmions [1] are prominent non-colinear spin configurations [2–7], which are observed in a variety of noncentrosymmetric materials [8], e.g. MnSi [9–20], Fe_{1-x}Co_xSi [21–31], FeGe [32–39], and Mn_{1-x}Fe_xGe [40–43]. They can be stabilized at finite temperatures and driven by extremely low current densities [44–47]. Due to their high mobility and stability, skyrmions have been a promising platform for next-generation magnetic memory devices [48–60].

The dynamics of skyrmions are governed by the Landau-Lifshitz-Gilbert (LLG) equation. A conventional way to simplify this equation is by using Thiele's method [61, 62]. This approach treats a skyrmion as a rigid particle [63] described by a two-dimension position vector $\mathbf{r}(t)$. As a result, the LLG equation reduces to a first-order differential equation in terms of $\dot{\mathbf{r}}(t)$. The reduced equation allows us to describe the current-induced motion of the skyrmion [64–66]. Experimental and theoretical studies have shown that, in response to an applied electric current density \mathbf{j} , skyrmions acquire velocities with components both parallel and perpendicular to \mathbf{j} . The latter effect is known as the skyrmion Hall effect [67–71].

The fact that the Thiele equation is first-order in the derivative $\dot{\mathbf{r}}(t)$ is usually interpreted as the absence of skyrmion mass, i.e. $m_{\text{sk}} = 0$. However, it has been shown that skyrmion mass can effectively be generated [72–75] due to the deformation of its shape. Skyrmion mass could have nontrivial implications for their current-induced dynamics. The purpose of this work is to point out that skyrmion mass is generically generated when skyrmions are confined to quasi-one-dimensional geometries (1D). The mass arises due to the combined effects of the skyrmion Hall effect and the system's elasticity. To date, there are two established approaches to confining skyrmions to 1D: using

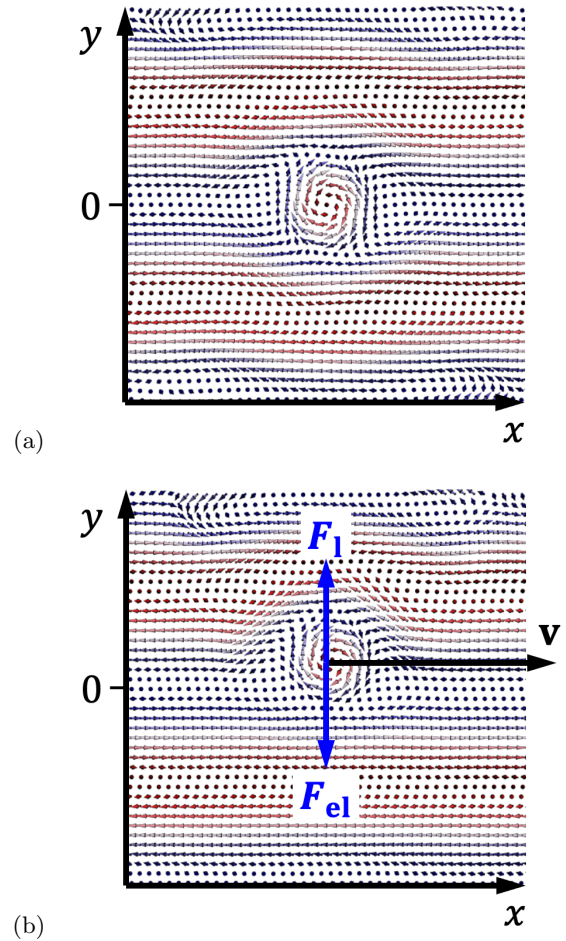


Figure 1. Graphical representation of the system. (a) A skyrmion confined inside a helical lane at rest. (b) A finite current density $\mathbf{j} \propto \hat{x}$ pushes the skyrmion with finite velocity $\mathbf{v} \propto \hat{x}$ along the lanes. The skyrmion shifts to a new equilibrium vertical position y , where the Lorentz force $F_L \propto v$ is balanced out by the elastic force $F_{el} \propto y$ produced by the deformed lane. Since $F_{el} = F_L$, the elastic potential energy scales as $U_{el} \propto y^2 \propto v^2$, which can be interpreted as a kinetic energy giving rise to the skyrmion inertia.

* Koichiro.Takahashi@unh.edu

† pershoguba@gmail.com

‡ Jiadong.Zang@unh.edu

helical backgrounds [76–83] or using magnetic nanostripes [50, 59, 84–89]. In this work, we focus on the

former scenario, however the results are equally applicable to the latter.

Consider a skyrmion nucleated inside the helical lanes [77–82] illustrated in Fig. 1. At rest, the skyrmion occupies a symmetric position ($y = 0$) between the two elastic helical lanes as shown in Fig. 1(a). At finite horizontal velocity v , as illustrated in Fig. 1(b), the skyrmion experiences the Lorentz force F_L due to the skyrmion Hall effect, which pushes the skyrmion along the positive y -axis. The helical lane acts as an elastic rubber band obstructing the skyrmion motion along y -axis. In response to the pressure from the skyrmion, the top lane deforms and pushes back with the elastic Hooke's force F_{el} . The skyrmion finds a new equilibrium position $y \neq 0$, where the Lorentz and elastic force balance each other $F_L = F_{el}$. Since the former force is proportional to the horizontal velocity $F_L \propto v$, whereas the latter force is proportional to the vertical displacement $F_{el} \propto y$, we conclude that $y \propto v$. So, the potential energy of elastic deformation is proportional to the square of velocity $U_{el} \propto y^2 \propto v^2$ and, therefore, can be interpreted as a kinetic energy leading to skyrmion inertia. The same phenomenology applies to skyrmions constricted within narrow nanoribbons [84–89], as long as the skyrmions are repelled from the nanoribbon's edge but not annihilated by it [65]. Real materials include impurities and disorders, which will cause skyrmion pinning at low current densities [90, 91]. For this reason, we include a simplified disorder potential in our model. We note that a similar mass generation mechanism was discussed in 2D nanodisc geometries [74, 92–95].

Below, we analyze the current-driven dynamics of a skyrmion confined to a quasi-1D lane by using the Thiele equation derived in Sec. II. In Sec. III, we derive the non-zero skyrmion mass m_{sk} . In Sec. IV, we apply our formalism to a simplified periodic model of the disorder. We find that skyrmion dynamics can be classified by a parameter \tilde{m}_{sk} representing a dimensionless skyrmion mass, given by Eq. (15). We identify two regimes for the skyrmion dynamics: of the (overdamped) small mass $\tilde{m}_{sk} \ll 1$ and the (underdamped) large mass $\tilde{m}_{sk} \gg 1$ regimes. In the latter regime, we show that the skyrmion dynamics could exhibit hysteresis in v_{sk} -vs- j graph akin to a similar behavior in Josephson junctions [96].

II. EQUATION OF SKYRMION MOTION: THIELE EQUATION

To analyze the dynamics of the magnetization $\mathbf{M}(\mathbf{r}, t)$ driven by the electric current density \mathbf{j} , the standard classical starting point is the Landau-Gilbert-Lifshitz (LLG) equation

$$\begin{aligned} \frac{\partial \mathbf{M}}{\partial t} = & \gamma \mathbf{B}^{\text{eff}} \times \mathbf{M} + \frac{\alpha}{M} \mathbf{M} \times \frac{\partial \mathbf{M}}{\partial t} \\ & + \frac{pa^3}{2eM} (\mathbf{j} \cdot \nabla) \mathbf{M} - \frac{pa^3\beta}{2eM^2} [\mathbf{M} \times (\mathbf{j} \cdot \nabla) \mathbf{M}]. \end{aligned} \quad (1)$$

For simplicity, we assume a planar geometry with $\mathbf{r} = (x, y)$ representing two-dimensional (2D) coordinates and $\mathbf{M} = (M_x, M_y, M_z)$ is a three-dimensional (3D) magnetization vector. The first term ($\propto \gamma$) on the right-hand side describes the gyromagnetic coupling with local magnetic field $\mathbf{B}^{\text{eff}}(\mathbf{r}, t)$, which can be derived from the spin Hamiltonian of the system [65]. The second term ($\propto \alpha$) describes the Gilbert damping [97] and produces friction. The third and fourth terms in Eq. (1) are known as the spin-transfer torques (STT) [98]. They describe the coupling with electric current density \mathbf{j} .

While the partial differential equation (1) is amenable for numerical integration, an adequate approximate solution can be obtained by Thiele's approach [61]. In this approach, it is assumed that the skyrmion can be treated as a rigid particle. So the magnetization dynamics may be approximated by an ansatz

$$\mathbf{M}(\mathbf{r}', t) = \mathbf{M}[\mathbf{r}' - \mathbf{r}(t)], \quad (2)$$

where $\mathbf{r}(t) = [x(t), y(t)]$ represents the time-dependent 2D position of the skyrmion. Substituting Eq. (2) into Eq. (1) and it reduces to a first-order differential equation

$$\mathcal{G} \hat{\mathbf{z}} \times (\mathbf{u} - \dot{\mathbf{r}}) + \mathcal{D} (\beta \mathbf{u} - \alpha \dot{\mathbf{r}}) - \nabla U(\mathbf{r}) = \mathbf{0} \quad (3)$$

in $\mathbf{r}(t)$. The constants α and β carry over from Eq. (1). The vector $\mathbf{u} = -\frac{pa^3}{2eM} \mathbf{j}$ is conventionally interpreted as the velocity of spins conducted by itinerant electrons. The two dimensionless constants

$$\begin{aligned} \mathcal{G} &= \int d^2r \hat{\Omega} \cdot \left(\frac{\partial \hat{\Omega}}{\partial x} \times \frac{\partial \hat{\Omega}}{\partial y} \right) = 4\pi, \quad \hat{\Omega} = \frac{\mathbf{M}}{M}, \\ \mathcal{D} &= \frac{1}{2} \int d^2r \left[\left(\frac{\partial \hat{\Omega}}{\partial x} \right)^2 + \left(\frac{\partial \hat{\Omega}}{\partial y} \right)^2 \right], \end{aligned}$$

describe the geometry of the skyrmion configuration. The constant \mathcal{G} represents the topological number of the skyrmion, which is independent of small deformations of the skyrmion shape caused by its motion. In contrast, constant \mathcal{D} may depend on the skyrmion shape, but that effect is not essential for the discussion below. The phenomenological potential energy $U(\mathbf{r})$ is added to account for the effects of the disorder and the confinement by helical lanes. Note that $U(\mathbf{r})$ has unconventional units of $\text{length}^2/\text{time}$.

A notable feature is that Eq. (3) contains the first-order $\dot{\mathbf{r}}$ but not the second-order $\ddot{\mathbf{r}}$ derivative. This fact is usually interpreted in literature as the absence of skyrmion mass. Nevertheless, as shown below, the skyrmion mass m_{sk} is effectively generated due to the combined effects of the skyrmion Hall effect and the elasticity of helical lanes.

III. SKYRMION MASS

The potential $U(\mathbf{r})$ appearing in Eq. (3) accounts both for helical lanes, illustrated in Fig. 1, and the dis-

order experienced by the skyrmion. To proceed further, we make a simplifying assumption that the potential is separable

$$U(\mathbf{r}) = U_{\text{hel}}(y) + U_{\text{dis}}(x) \quad (4)$$

in x and y variables. The first term $U_{\text{hel}}(y)$ describes the confinement potential due to helical lanes. At small y , the potential is parabolic

$$U_{\text{hel}}(y) = \frac{1}{2}ky^2 \quad (5)$$

where k is the corresponding elasticity constant. Assuming that the helical potential (5) is sufficiently stiff, it confines the skyrmion within one helical lane $|y| < w$, where w is the lane width. Consequently, the skyrmion is subject to the disorder only within the corresponding

helical lane, and we can model the disorder potential as a purely x -dependent function $U_{\text{dis}}(x)$.

We assume that the current \mathbf{j} is pointing along the helical lanes

$$\mathbf{u} = u \hat{x}. \quad (6)$$

Substituting Eqs. (4), (5), and (6) into the Thiele equation (3) and writing it in components, we obtain a pair of first-order differential equations

$$\begin{aligned} \mathcal{G} \dot{y} + \mathcal{D}(\beta u - \alpha \dot{x}) - \frac{\partial U_{\text{dis}}(x)}{\partial x} &= 0, \\ \mathcal{G}(u - \dot{x}) - \mathcal{D} \alpha \dot{y} - ky &= 0. \end{aligned} \quad (7)$$

Eq. (7) can be reduced to a single second-order differential equation on $x(t)$. Differentiating Eq. (7) over time, we obtain a system of four equations in total. Eliminating the variables $y(t)$, we arrive at a second-order differential equation on $x(t)$ (See Appendix. A)

$$\left(\frac{\mathcal{G}^2 + \mathcal{D}^2 \alpha^2}{k} \right) \ddot{x} + \mathcal{D} \alpha \left(1 + \frac{1}{k} \frac{\partial^2 U_{\text{dis}}(x)}{\partial x^2} \right) \dot{x} - \left(\frac{\mathcal{G}^2 + \mathcal{D}^2 \alpha \beta}{k} \right) \dot{u} - \mathcal{D} \beta u + \frac{\partial U_{\text{dis}}(x)}{\partial x} = 0. \quad (8)$$

Let us comment on the terms appearing in Eq. (8), which is the main focus of this paper. The equation has a form of Newton's 2nd law with the combination

$$m_{\text{sk}} = \frac{\mathcal{G}^2 + \mathcal{D}^2 \alpha^2}{k} \quad (9)$$

playing the role of skyrmion mass. In realistic experimental situations, the Gilbert damping is small $\alpha \ll 1$, so the skyrmion mass $m_{\text{sk}} \approx \mathcal{G}^2/k$ is determined by the skyrmion Hall effect \mathcal{G} and the elasticity constant k , and the mass has units of time. The last three terms in Eq. (8) represent the three sources of driving force acting on the skyrmion. The term $\partial U_{\text{dis}}(x)/\partial x$ describes the effect of the disorder. The two terms $\propto u$ and $\propto \dot{u}$ represent the force produced by the electric current $u(t)$, which we henceforth refer to as the ‘‘push force’’. The second term $\propto \dot{x}$ describes a variable friction force experienced by the interstitial skyrmion.

Let us comment on the applicability of our approach. Our model relies on quadratic approximation (5) for the potential induced by helical lanes. So, the model is not applicable, when that approximation fails, i.e. where the vertical displacement y is of the order of interlane distance w , i.e. $y \sim w$. This will occur at some maximum push force u_{max} causing the interstitial skyrmion to be pressed too hard against the helical lanes due to the skyrmion Hall effect. The value of u_{max} can be estimated by dropping the disorder potential from Eq. (7), setting $y = w$, $\dot{y} = 0$, ignoring the disorder term due to

the large current, and solving for u

$$u_{\text{max}} \sim \frac{\alpha}{\alpha - \beta} \frac{kw}{\mathcal{G}}. \quad (10)$$

We expect that our approach is applicable at push force below $u < u_{\text{max}}$. In practice, experiments show that large current densities j cause skyrmions to annihilate or transform into meron pairs [78, 86].

IV. SKYRMION DYNAMICS IN A CASE OF A SIMPLIFIED DISORDER POTENTIAL

The purpose of this section is to investigate skyrmion dynamics for a simple model of the disorder, however, all conclusions carry over to more realistic models. (i) We assume that $u(t)$ is varied slowly, so \dot{u} in Eq. (8) can be neglected. (ii) We assume that stiffness of helices k is much greater than that of the disorder $\partial^2 U_{\text{dis}}(x)/\partial x^2$, so their ratio $\partial^2 U_{\text{dis}}(x)/k\partial x^2$ in the friction term can be neglected. (iii) Finally, we model the disorder potential as a periodic function [99, 100]

$$U_{\text{dis}}(x) = -U_0 \cos Kx, \quad (11)$$

where U_0 describes the disorder strength, and $\tilde{m}_{\text{sk}} = \frac{2\pi}{K}$ represents a typical spatial scale over which the disorder varies. Equivalently, the wave number K characterizes the average density of impurities. Then, Eq. (8) reduces to

$$m_{\text{sk}} \ddot{x} + \mathcal{D} \alpha \dot{x} - \mathcal{D} \beta u + U_0 K \sin(Kx) = 0. \quad (12)$$

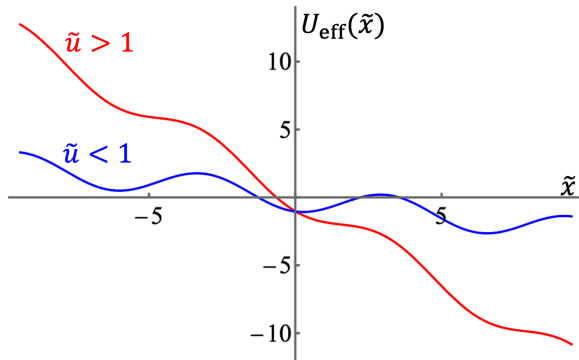


Figure 2. If the push force is large, i.e. $\tilde{u} > 1$, the washboard potential is monotonic causing the skyrmion to propagate. In contrast, if the push force is small, i.e. $\tilde{u} < 1$, the washboard potential is non-monotonic with minima, which could pin the skyrmion.

To analyze this equation, it is practical to switch to dimensionless variables denoted by “ \sim ”:

$$\tilde{x} = Kx, \quad \tilde{t} = \frac{t}{\mathcal{D}\alpha/U_0K^2}, \quad \tilde{u} = \frac{u}{U_0K/\mathcal{D}\beta}. \quad (13)$$

In the new variables, Eq. (12) simplifies to

$$\tilde{m}_{\text{sk}} \frac{d^2\tilde{x}}{d\tilde{t}^2} + \frac{d\tilde{x}}{d\tilde{t}} - \tilde{u} + \sin\tilde{x} = 0, \quad (14)$$

with a constant

$$\tilde{m}_{\text{sk}} = \frac{m_{\text{sk}}U_0K^2}{\alpha^2\mathcal{D}^2} \quad (15)$$

representing a dimensionless mass.

It is instructive to combine the last two terms of Eq. (14) into a single effective potential

$$\tilde{m}_{\text{sk}} \frac{d^2\tilde{x}}{d\tilde{t}^2} + \frac{d\tilde{x}}{d\tilde{t}} + \frac{\partial U_{\text{eff}}(\tilde{x})}{\partial\tilde{x}} = 0, \quad (16)$$

$$U_{\text{eff}}(\tilde{x}) = -\tilde{u}\tilde{x} - \cos\tilde{x}.$$

It is known as a washboard potential and has been extensively studied in the context of Josephson junctions [96, 101, 102]. The washboard potential consists of a linear term in \tilde{x} and a periodic potential due to the disorder as shown in Fig. 2. If the push force is larger than the disorder potential, i.e. $\tilde{u} > 1$, the potential is a monotonously decreasing function causing the skyrmion to roll down the hill. In contrast, if the push force is smaller, i.e. $\tilde{u} < 1$, the potential becomes non-monotonic and develops local minima as shown by the blue curve. In the absence of skyrmion mass, i.e. $m_{\text{sk}} = 0$, the potential minima inevitably pin the skyrmion. However, in the presence of the skyrmion mass, i.e. $m_{\text{sk}} \neq 0$, the skyrmion could sustain a propagating mode due to its inertia allowing the skyrmion to overcome potential barriers.

The discussion below follows a known behavior in Josephson junctions [96], according to which, the dynamics can be classified as either overdamped friction-dominated $\tilde{m}_{\text{sk}} \ll 1$ or underdamped mass-dominated $\tilde{m}_{\text{sk}} \gg 1$.

A. Overdamped regime $\tilde{m}_{\text{sk}} \ll 1$

We set $\tilde{m}_{\text{sk}} = 0$, so Eq. (12) becomes

$$\frac{d\tilde{x}}{d\tilde{t}} = \tilde{u} - \sin\tilde{x}. \quad (17)$$

It implies that the velocity of the skyrmion is a periodic function of \tilde{x} . Integrating this first-order differential equation (see Appendix. B), we compute the velocity averaged over time

$$\langle \tilde{v}_{\text{sk}} \rangle \equiv \left\langle \frac{d\tilde{x}}{d\tilde{t}} \right\rangle_t = \begin{cases} 0 & \text{if } \tilde{u} \leq 1, \\ \sqrt{\tilde{u}^2 - 1} & \text{if } \tilde{u} > 1. \end{cases} \quad (18)$$

At low push force $\tilde{u} \leq 1$, the skyrmion is pinned by the minima in the washboard potential (16). Above the critical depinning force $\tilde{u} > 1$, the minima of the washboard potential (16) disappear, and it becomes a monotonic function causing the skyrmion to propagate with finite velocity.

B. Underdamped regime $\tilde{m}_{\text{sk}} \gg 1$.

The discussion above shows that massless skyrmion is pinned if the washboard potential contains barriers at $\tilde{u} < 1$. Below, we show that, in the opposite limit of large mass $\tilde{m}_{\text{sk}} \gg 1$, the skyrmion can overcome the barriers using its inertia. This will cause lower critical depinning currents $\tilde{u}_{\text{cr}} < 1$.

To proceed further, we move the second and the third term to the right-hand side of Eq. (14), multiply the whole equation by $d\tilde{x}/d\tilde{t}$ and integrate:

$$\frac{1}{2}\tilde{m}_{\text{sk}}\tilde{v}_{\text{sk}}^2(\tilde{x}) - \cos\tilde{x} - (\varepsilon_0 - 1) = \int_0^{\tilde{x}} dx [\tilde{u} - \tilde{v}_{\text{sk}}(x)]. \quad (19)$$

Here, we switched to a new independent variable \tilde{x} instead of \tilde{t} and denoted $d\tilde{x}/d\tilde{t} \equiv \tilde{v}_{\text{sk}}$. Eq. (19) has a transparent physical meaning. It relates the change of the mechanical energy (on the left-hand side) to the work done by the push $\propto \tilde{u}$ and the friction $\propto \tilde{v}_{\text{sk}}(\tilde{x})$ forces (on the right-hand side). The constant of integration ε_0 represents the initial kinetic energy of the skyrmion.

Eq. (19) can be viewed as an integral equation on the unknown function $\tilde{v}_{\text{sk}}(\tilde{x})$. We focus on a periodic solution [101], where the net work in the right-hand side of Eq. (19) is zero over one period

$$\int_0^{2\pi} d\tilde{x} [\tilde{u} - \tilde{v}_{\text{sk}}(\tilde{x})] = 0. \quad (20)$$

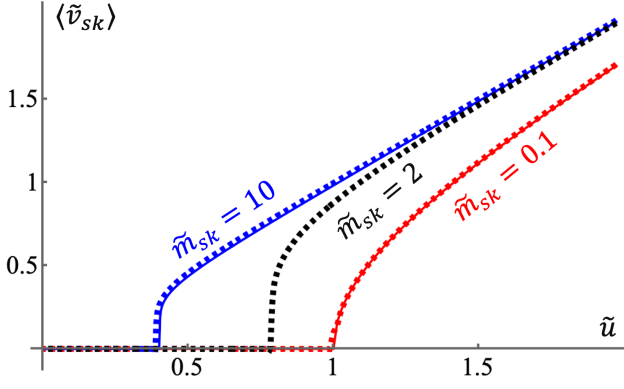


Figure 3. The \tilde{v}_{sk} -vs- \tilde{u} curves for a skyrmion in a quasi-1D lane. The dashed lines correspond to the numerical solutions of the differential equation (14), whereas the solid lines correspond to the analytical expressions (18) and (24)

Integrating the term $\propto \tilde{u}$ allows us to cast Eq. (20) in a form

$$\tilde{u} = \frac{1}{2\pi} \int_0^{2\pi} d\tilde{x} \tilde{v}_{sk}(\tilde{x}). \quad (21)$$

In the limit of small friction $\tilde{m}_{sk} \gg 1$, on the other hand, the mechanical energy [the left-hand side of Eq. (19)] is conserved $\frac{1}{2}\tilde{m}_{sk}\tilde{v}_{sk}^2(\tilde{x}) - \cos\tilde{x} - \varepsilon_*(\tilde{u}) + 1 = 0$ to a good accuracy at arbitrary \tilde{x} . Here $\varepsilon_*(\tilde{u})$ denotes the kinetic energy of the periodic orbit that replaced the arbitrary constant ε_0 . Solving the latter algebraic equation in terms of velocity, one finds

$$\tilde{v}_{sk}(\tilde{x}) = \sqrt{\frac{2}{\tilde{m}_{sk}} \left(\varepsilon_*(\tilde{u}) - 2 \sin^2 \frac{\tilde{x}}{2} \right)}. \quad (22)$$

Substituting it into Eq. (21), we obtain

$$\tilde{u} = \frac{1}{\pi} \sqrt{\frac{8\varepsilon_*(\tilde{u})}{\tilde{m}_{sk}}} E \left(\sqrt{\frac{2}{\varepsilon_*(\tilde{u})}} \right), \quad (23)$$

using a complete elliptic integral of the second kind $E(z)$ [103]. This implicit equation can be solved numerically to find the energy $\varepsilon_*(\tilde{u})$ corresponding to push force \tilde{u} . If $\varepsilon_*(\tilde{u})$ is known, one can substitute it back into Eq. (22) and compute the velocity averaged over time

$$\langle \tilde{v}_{sk} \rangle = \begin{cases} 0 & \text{if } \tilde{u} < \tilde{u}_{cr} \\ \sqrt{\frac{\varepsilon_*(\tilde{u})}{2\tilde{m}_{sk}}} \cdot \frac{\pi}{K\left(\sqrt{\frac{2}{\varepsilon_*(\tilde{u})}}\right)} & \text{if } \tilde{u} > \tilde{u}_{cr}. \end{cases} \quad (24)$$

where $\tilde{u}_{cr} = \frac{4}{\pi} \frac{1}{\sqrt{\tilde{m}_{sk}}}$ is a critical push force at which depinning occurs, and $K(z)$ is a complete elliptic integral of the first kind. A pair of equations (23) and (24) should be used to compute the \tilde{v}_{sk} -vs- \tilde{u} curves numerically.

Now, let us compute the \tilde{v}_{sk} -vs- \tilde{u} curves for a range of parameters \tilde{m}_{sk} corresponding to friction-dominated

$\tilde{m}_{sk} \ll 1$ and mass-dominated $\tilde{m}_{sk} \gg 1$ regimes and present the results in Fig. 3. We solve the differential equation (14) numerically, average the velocity over time $\langle \tilde{v}_{sk} \rangle = \langle \dot{\tilde{x}} \rangle_t$ and plot it in dashed lines. For comparison, the analytical expressions (18) and (24), plotted in solid lines, agree with the numerical results well. At large current \tilde{u} , all curves approach the same asymptote $\langle \tilde{v}_{sk} \rangle = \tilde{u}$. The main effect of skyrmion inertia appears near depinning. (i) In the massless regime, $\tilde{m}_{sk} = 0$, the critical depinning current is set by the disorder potential $\tilde{u}_{cr} = 1$ (or $u_{cr} = \frac{U_0 K}{D\beta}$ in the dimensional units). The velocity grows as a square root $\tilde{v}_{sk}(\delta\tilde{u}) \sim \sqrt{2\delta\tilde{u}}$ close to depinning $\delta\tilde{u} = \tilde{u} - \tilde{u}_{cr} \ll 1$. (ii) In the large mass limit $\tilde{m}_{sk} \gg 1$, the critical depinning current is lowered to $\tilde{u}_{cr} = \frac{4}{\pi\sqrt{\tilde{m}_{sk}}}$ ($u_{cr} = \frac{4\alpha}{\pi\beta} \sqrt{\frac{U_0}{\tilde{m}_{sk}}}$ in the dimensional units). The velocity exhibits a strongly non-analytic step-like behavior. It can be expressed $\tilde{v}_{sk}(\delta\tilde{u}) \sim \frac{1}{\sqrt{\tilde{m}_{sk} W_{-1}(-\sqrt{\tilde{m}_{sk} \delta\tilde{u}})}}$, via a Lambert function $W(x)$ [104]. Such a sharp step-wise onset of the velocity near depinning may serve as an indicator of the underdamped regime $\tilde{m}_{sk} \gg 1$. A similar step-like behavior was recently observed in Ref. [86], which we take as a strong indication that $\tilde{m}_{sk} \gg 1$ in that system.

C. Hysteresis in the \tilde{v}_{sk} -vs- \tilde{u} curves at $\tilde{m}_{sk} \gg 1$

Another noteworthy feature of massive dynamics $\tilde{m}_{sk} \gg 1$ is hysteresis of the \tilde{v}_{sk} -vs- \tilde{u} curve, which we consider below. For the discussion below, let us summarize the two critical push forces, found above, as

$$\begin{aligned} \tilde{u}_{cr}^{(1)} &= 1 \\ \tilde{u}_{cr}^{(2)} &= \frac{4}{\pi\sqrt{\tilde{m}_{sk}}}, \end{aligned} \quad (25)$$

where $\tilde{u}_{cr}^{(1)} > \tilde{u}_{cr}^{(2)}$ for $\tilde{m}_{sk} \gg 1$. According to Fig. 2, the push forces above the first critical current $\tilde{u} > \tilde{u}_{cr}^{(1)}$ correspond to monotonically decreasing potential causing the skyrmion to propagate with a finite velocity. For lower push forces in the window between the two critical values $\tilde{u}_{cr}^{(1)} > \tilde{u} > \tilde{u}_{cr}^{(2)}$, the washboard potential contains local minima and admits two solutions. (i) One solution corresponds to a stationary skyrmion parked at one of the local minima, e.g. $\tilde{x}(t) = 0$. (ii) Another solution, which was discussed in Sec. IV B above, corresponds to a propagating solution. Whether the skyrmion takes either of the two solutions (i) or (ii), depends on the history of $\tilde{u}(t)$, which leads to hysteresis. Specifically, we consider the following driving protocol for the push force

$$\tilde{u}(t) = 1.5 \left[1 - \left| \frac{2t}{T} - 1 \right| \right] \quad (26)$$

over the time interval $0 < t < T$. The protocol $\tilde{u}(t)$ is illustrated in Fig. 4(a). By taking sufficiently large T compared to the fluctuation time scale by the disorder,

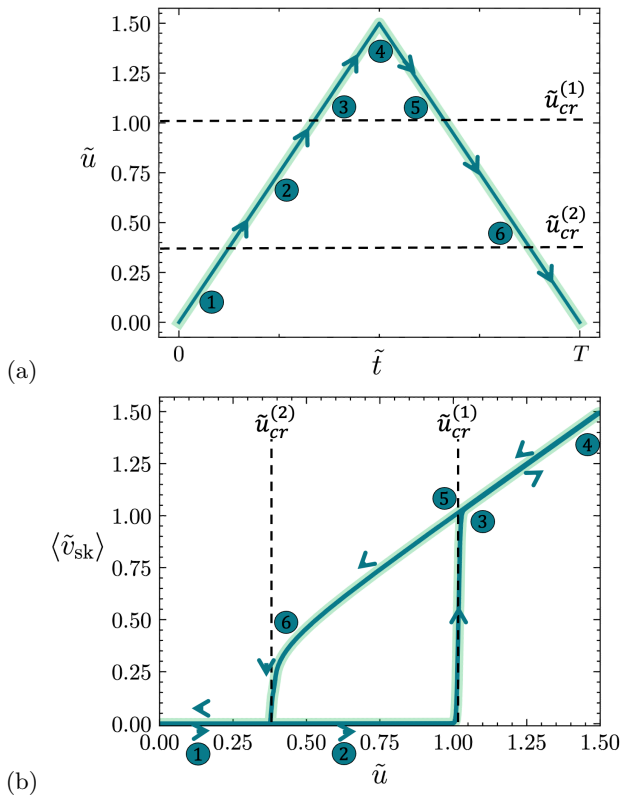


Figure 4. (a) Protocol for changing the push force $\tilde{u}(\tilde{t})$ leading to hysteresis: the push force is slowly ramped up and then gradually decreased back to zero over some large time T . (b) The numerically calculated skyrmion velocity $\langle \tilde{v}_{\text{sk}} \rangle$ exhibits hysteresis. The arrows and the numerical labels can be used as a guide to the eye to compare the two panels.

the push force is slowly ramped up from 0 to a maximum value of $\tilde{u} = 1.5 > \tilde{u}_{\text{cr}}^{(1)}$ followed by a slow reduction back to 0. We substitute Eq. (26) into the Eq. (14), and solve it numerically and average skyrmion velocity $\langle \tilde{v}_{\text{sk}} \rangle$ over a sufficiently long-time compared with the oscillation time of the skyrmion but small compared to T . The $\langle \tilde{v}_{\text{sk}} \rangle$ -vs- \tilde{u} curve has hysteresis as shown in Fig. 4(b). Initially, at

$0 < t < T/2$, the stationary skyrmion remains pinned by the minima of the washboard potential at $\tilde{u} < \tilde{u}_{\text{cr}}^{(1)}$. Eventually, \tilde{u} surpasses $\tilde{u}_{\text{cr}}^{(1)}$ and the minima disappear, leading to an abrupt jump to the propagating solution. For later times, at $T/2 < t < T$, the push force decreases, but the skyrmion sustains a non-zero velocity $\langle \tilde{v}_{\text{sk}} \rangle$ even for low push forces at $\tilde{u}_{\text{cr}}^{(2)} < \tilde{u} < \tilde{u}_{\text{cr}}^{(1)}$ due to its inertia. Eventually, at $\tilde{u} < \tilde{u}_{\text{cr}}^{(2)}$, the potential minima are strong enough to pin the skyrmion.

V. CONCLUSION

In this work, we show that skyrmions confined to quasi-1D geometries generically acquire a non-zero mass. We investigate the dynamics of a massive skyrmion pushed by electric current \tilde{u} in 1D. We find that the dynamics can be classified by a dimensionless parameter \tilde{m}_{sk} , given by Eq. (15). In the overdamped regime $\tilde{m}_{\text{sk}} \ll 1$, the skyrmion velocity scales as a square root $\tilde{v}_{\text{sk}} \propto \sqrt{\tilde{u} - \tilde{u}_{\text{cr}}}$ close to depinning current \tilde{u}_{cr} . In contrast, in the overdamped regime, the skyrmion velocity exhibits a sharp step-like onset at \tilde{u}_{cr} as shown in Fig. 3. A similar step-like feature was recently observed in Ref. [86]. Remarkably, in the underdamped regime $\tilde{m}_{\text{sk}} \gg 1$, non-zero skyrmion mass could lead to hysteresis of the current-driven skyrmion dynamics, see Fig. 4. The experimental realization of hysteresis in the dynamics of skyrmion confined in one dimension could have applications in skyrmion-based memory architectures.

ACKNOWLEDGEMENTS

This work was supported by the Office of Basic Energy Sciences, Division of Materials Sciences and Engineering, U.S. Department of Energy, under Award No. DE-SC0020221. K.Takahashi was supported by the Summer Undergraduate Research Fellowships at the Hamel Center for Undergraduate Research of the University of New Hampshire.

-
- [1] T. Skyrme, A unified field theory of mesons and baryons, *Nuclear Physics* **31**, 556 (1962).
 - [2] A. N. Bogdanov and D. Yablonskii, Thermodynamically stable “vortices” in magnetically ordered crystals. the mixed state of magnets, *Zh. Eksp. Teor. Fiz* **95**, 178 (1989).
 - [3] A. Bogdanov and A. Hubert, Thermodynamically stable magnetic vortex states in magnetic crystals, *Journal of Magnetism and Magnetic Materials* **138**, 255 (1994).
 - [4] U. K. Rößler, A. N. Bogdanov, and C. Pfleiderer, Spontaneous skyrmion ground states in magnetic metals, *Nature* **442**, 797 (2006).
 - [5] C. Back, V. Cros, H. Ebert, K. Everschor-Sitte, A. Fert, M. Garst, T. Ma, S. Mankovsky, T. L. Monchisky, M. Mostovoy, N. Nagaosa, S. S. P. Parkin, C. Pfleiderer, N. Reyren, A. Rosch, Y. Taguchi, Y. Tokura, K. von Bergmann, and J. Zang, The 2020 skyrmionics roadmap, *Journal of Physics D: Applied Physics* **53**, 363001 (2020).
 - [6] B. Göbel, I. Mertig, and O. A. Tretiakov, Beyond skyrmions: Review and perspectives of alternative magnetic quasiparticles, *Physics Reports* **895**, 1 (2021).
 - [7] W. Jiang, G. Chen, K. Liu, J. Zang, S. G. te Velthuis, and A. Hoffmann, Skyrmions in magnetic multilayers,

- Physics Reports **704**, 1 (2017).
- [8] Y. Tokura and N. Kanazawa, Magnetic skyrmion materials, *Chemical Reviews* **121**, 2857 (2021).
 - [9] S. Mühlbauer, B. Binz, F. Jonietz, C. Pfleiderer, A. Rosch, A. Neubauer, R. Georgii, and P. Böni, Skyrmion lattice in a chiral magnet, *Science* **323**, 915 (2009).
 - [10] Y. Ishikawa, K. Tajima, D. Bloch, and M. Roth, Helical spin structure in manganese silicide MnSi, *Solid State Communications* **19**, 525 (1976).
 - [11] Y. Ishikawa and M. Arai, Magnetic phase diagram of MnSi near critical temperature studied by neutron small angle scattering, *Journal of the Physical Society of Japan* **53**, 2726 (1984).
 - [12] B. Lebech, P. Harris, J. Skov Pedersen, K. Mortensen, C. Gregory, N. Bernhoeft, M. Jermy, and S. Brown, Magnetic phase diagram of MnSi, *Journal of Magnetism and Magnetic Materials* **140-144**, 119 (1995), international Conference on Magnetism.
 - [13] C. Pfleiderer, D. Reznik, L. Pintschovius, H. v. Löhneysen, M. Garst, and A. Rosch, Partial order in the non-Fermi-liquid phase of MnSi, *Nature* **427**, 227 (2004).
 - [14] S. V. Grigoriev, V. A. Dyadkin, E. V. Moskvina, D. Lamago, T. Wolf, H. Eckerlebe, and S. V. Maleyev, Helical spin structure of $Mn_{1-y}Fe_ySi$ under a magnetic field: Small angle neutron diffraction study, *Phys. Rev. B* **79**, 144417 (2009).
 - [15] T. Adams, S. Mühlbauer, C. Pfleiderer, F. Jonietz, A. Bauer, A. Neubauer, R. Georgii, P. Böni, U. Keiderling, K. Everschor, M. Garst, and A. Rosch, Long-range crystalline nature of the skyrmion lattice in MnSi, *Phys. Rev. Lett.* **107**, 217206 (2011).
 - [16] H. Du, J. P. DeGrave, F. Xue, D. Liang, W. Ning, J. Yang, M. Tian, Y. Zhang, and S. Jin, Highly stable skyrmion state in helimagnetic MnSi nanowires, *Nano Letters* **14**, 2026 (2014).
 - [17] X. Yu, J. P. DeGrave, Y. Hara, T. Hara, S. Jin, and Y. Tokura, Observation of the magnetic skyrmion lattice in a MnSi nanowire by Lorentz TEM, *Nano Letters* **13**, 3755 (2013).
 - [18] A. Tonomura, X. Yu, K. Yanagisawa, T. Matsuda, Y. Onose, N. Kanazawa, H. S. Park, and Y. Tokura, Real-space observation of skyrmion lattice in helimagnet MnSi thin samples, *Nano Letters* **12**, 1673 (2012).
 - [19] T. Nakajima, H. Oike, A. Kikkawa, E. P. Gilbert, N. Booth, K. Kakurai, Y. Taguchi, Y. Tokura, F. Kagawa, and T. Hisa Arima, Skyrmion lattice structural transition in MnSi, *Science Advances* **3**, e1602562 (2017).
 - [20] M. Janoschek, M. Garst, A. Bauer, P. Krautscheid, R. Georgii, P. Böni, and C. Pfleiderer, Fluctuation-induced first-order phase transition in Dzyaloshinskii-Moriya helimagnets, *Phys. Rev. B* **87**, 134407 (2013).
 - [21] X. Z. Yu, Y. Onose, N. Kanazawa, J. H. Park, J. H. Han, Y. Matsui, N. Nagaosa, and Y. Tokura, Real-space observation of a two-dimensional skyrmion crystal, *Nature* **465**, 901 (2010).
 - [22] J. Beille, J. Voiron, and M. Roth, Long period helimagnetism in the cubic b20 $Fe_xCo_{1-x}Si$ and $Co_xMn_{1-x}Si$ alloys, *Solid State Communications* **47**, 399 (1983).
 - [23] K. Ishimoto, Y. Yamaguchi, J. Suzuki, M. Arai, M. Furusaka, and Y. Endoh, Small-angle neutron diffraction from the helical magnet $Fe_{0.8}Co_{0.2}Si$, *Physica B: Condensed Matter* **213-214**, 381 (1995).
 - [24] S. V. Grigoriev, V. A. Dyadkin, D. Menzel, J. Schoenes, Y. O. Chetverikov, A. I. Okorokov, H. Eckerlebe, and S. V. Maleyev, Magnetic structure of $Fe_{1-x}Co_xSi$ in a magnetic field studied via small-angle polarized neutron diffraction, *Phys. Rev. B* **76**, 224424 (2007).
 - [25] S. V. Grigoriev, D. Chernyshov, V. A. Dyadkin, V. Dmitriev, S. V. Maleyev, E. V. Moskvina, D. Menzel, J. Schoenes, and H. Eckerlebe, Crystal handedness and spin helix chirality in $Fe_{1-x}Co_xSi$, *Phys. Rev. Lett.* **102**, 037204 (2009).
 - [26] Y. Onose, N. Takeshita, C. Terakura, H. Takagi, and Y. Tokura, Doping dependence of transport properties in $Fe_{1-x}Co_xSi$, *Phys. Rev. B* **72**, 224431 (2005).
 - [27] W. Münzer, A. Neubauer, T. Adams, S. Mühlbauer, C. Franz, F. Jonietz, R. Georgii, P. Böni, B. Pedersen, M. Schmidt, A. Rosch, and C. Pfleiderer, Skyrmion lattice in the doped semiconductor $Fe_{1-x}Co_xSi$, *Phys. Rev. B* **81**, 041203 (2010).
 - [28] A. Bauer, M. Garst, and C. Pfleiderer, History dependence of the magnetic properties of single-crystal $Fe_{1-x}Co_xSi$, *Phys. Rev. B* **93**, 235144 (2016).
 - [29] L. J. Bannenberg, K. Kakurai, F. Qian, E. Lelièvre-Berna, C. D. Dewhurst, Y. Onose, Y. Endoh, Y. Tokura, and C. Pappas, Extended skyrmion lattice scattering and long-time memory in the chiral magnet $Fe_{1-x}Co_xSi$, *Phys. Rev. B* **94**, 104406 (2016).
 - [30] D. Morikawa, K. Shibata, N. Kanazawa, X. Z. Yu, and Y. Tokura, Crystal chirality and skyrmion helicity in MnSi and (Fe, Co)Si as determined by transmission electron microscopy, *Phys. Rev. B* **88**, 024408 (2013).
 - [31] C. Pfleiderer, T. Adams, A. Bauer, W. Biberacher, B. Binz, F. Birkelbach, P. Böni, C. Franz, R. Georgii, M. Janoschek, F. Jonietz, T. Keller, R. Ritz, S. Mühlbauer, W. Münzer, A. Neubauer, B. Pedersen, and A. Rosch, Skyrmion lattices in metallic and semiconducting B20 transition metal compounds, *Journal of Physics: Condensed Matter* **22**, 164207 (2010).
 - [32] B. Lebech, J. Bernhard, and T. Freltoft, Magnetic structures of cubic FeGe studied by small-angle neutron scattering, *Journal of Physics: Condensed Matter* **1**, 6105 (1989).
 - [33] M. Uchida, N. Nagaosa, J. P. He, Y. Kaneko, S. Iguchi, Y. Matsui, and Y. Tokura, Topological spin textures in the helimagnet FeGe, *Phys. Rev. B* **77**, 184402 (2008).
 - [34] X. Z. Yu, N. Kanazawa, Y. Onose, K. Kimoto, W. Z. Zhang, S. Ishiwata, Y. Matsui, and Y. Tokura, Near room-temperature formation of a skyrmion crystal in thin-films of the helimagnet FeGe, *Nature Materials* **10**, 106 (2011).
 - [35] H. Wilhelm, M. Baenitz, M. Schmidt, U. K. Rößler, A. A. Leonov, and A. N. Bogdanov, Precursor phenomena at the magnetic ordering of the cubic helimagnet FeGe, *Phys. Rev. Lett.* **107**, 127203 (2011).
 - [36] J. C. Gallagher, K. Y. Meng, J. T. Brangham, H. L. Wang, B. D. Esser, D. W. McComb, and F. Y. Yang, Robust zero-field skyrmion formation in FeGe epitaxial thin films, *Phys. Rev. Lett.* **118**, 027201 (2017).
 - [37] X. Zhao, C. Jin, C. Wang, H. Du, J. Zang, M. Tian, R. Che, and Y. Zhang, Direct imaging of magnetic field-driven transitions of skyrmion cluster states in FeGe nanodisks, *Proceedings of the National Academy*

- of *Sciences* **113**, 4918 (2016).
- [38] M. B. Venuti, X. S. Zhang, E. J. Lang, S. J. Addamane, H. Paik, P. Allen, P. Sharma, D. Muller, K. Hattar, T.-M. Lu, and S. Eley, Inducing a tunable skyrmion-antiskyrmion system through ion beam modification of FeGe films, *npj Spintronics* **2**, 16 (2024).
- [39] S. Budhathoki, A. Sapkota, K. M. Law, S. Ranjit, B. Nepal, B. D. Hoskins, A. S. Thind, A. Y. Borisevich, M. E. Jamer, T. J. Anderson, A. D. Koehler, K. D. Hobart, G. M. Stephen, D. Heiman, T. Mewes, R. Mishra, J. C. Gallagher, and A. J. Hauser, Room-temperature skyrmions in strain-engineered FeGe thin films, *Phys. Rev. B* **101**, 220405 (2020).
- [40] K. Shibata, X. Z. Yu, T. Hara, D. Morikawa, N. Kanazawa, K. Kimoto, S. Ishiwata, Y. Matsui, and Y. Tokura, Towards control of the size and helicity of skyrmions in helimagnetic alloys by spin-orbit coupling, *Nature Nanotechnology* **8**, 723 (2013).
- [41] J. Gayles, F. Freimuth, T. Schena, G. Lani, P. Mavropoulos, R. A. Duine, S. Blügel, J. Sinova, and Y. Mokrousov, Dzyaloshinskii-Moriya interaction and Hall effects in the skyrmion phase of $Mn_{1-x}Fe_xGe$, *Phys. Rev. Lett.* **115**, 036602 (2015).
- [42] T. Koretsune, N. Nagaosa, and R. Arita, Control of Dzyaloshinskii-Moriya interaction in $Mn_{1-x}Fe_xGe$: a first-principles study, *Scientific Reports* **5**, 13302 (2015).
- [43] T. Yokouchi, N. Kanazawa, A. Tsukazaki, Y. Kozuka, M. Kawasaki, M. Ichikawa, F. Kagawa, and Y. Tokura, Stability of two-dimensional skyrmions in thin films of $Mn_{1-x}Fe_xSi$ investigated by the topological Hall effect, *Phys. Rev. B* **89**, 064416 (2014).
- [44] N. Nagaosa and Y. Tokura, Topological properties and dynamics of magnetic skyrmions, *Nature Nanotechnology* **8**, 899 (2013).
- [45] F. Jonietz, S. Mühlbauer, C. Pfleiderer, A. Neubauer, W. Münzer, A. Bauer, T. Adams, R. Georgii, P. Böni, R. A. Duine, K. Everschor, M. Garst, and A. Rosch, Spin transfer torques in MnSi at ultralow current densities, *Science* **330**, 1648 (2010).
- [46] T. Schulz, R. Ritz, A. Bauer, M. Halder, M. Wagner, C. Franz, C. Pfleiderer, K. Everschor, M. Garst, and A. Rosch, Emergent electrodynamics of skyrmions in a chiral magnet, *Nature Physics* **8**, 301 (2012).
- [47] W. Wang, D. Song, W. Wei, P. Nan, S. Zhang, B. Ge, M. Tian, J. Zang, and H. Du, Electrical manipulation of skyrmions in a chiral magnet, *Nature Communications* **13**, 1593 (2022).
- [48] S. S. P. Parkin, M. Hayashi, and L. Thomas, Magnetic domain-wall racetrack memory, *Science* **320**, 190 (2008).
- [49] A. Fert, V. Cros, and J. Sampaio, Skyrmions on the track, *Nature Nanotechnology* **8**, 152 (2013).
- [50] X. Zhang, G. P. Zhao, H. Fangohr, J. P. Liu, W. X. Xia, J. Xia, and F. J. Morvan, Skyrmion-skyrmion and skyrmion-edge repulsions in skyrmion-based racetrack memory, *Scientific Reports* **5**, 7643 (2015).
- [51] S. Luo and L. You, Skyrmion devices for memory and logic applications, *APL Materials* **9**, 050901 (2021).
- [52] G. Yu, P. Upadhyaya, Q. Shao, H. Wu, G. Yin, X. Li, C. He, W. Jiang, X. Han, P. K. Amiri, and K. L. Wang, Room-temperature skyrmion shift device for memory application, *Nano Letters* **17**, 261 (2017).
- [53] R. Tomasello, E. Martinez, R. Zivieri, L. Torres, M. Carpentieri, and G. Finocchio, A strategy for the design of skyrmion racetrack memories, *Scientific Reports* **4**, 6784 (2014).
- [54] W. Koshibae, Y. Kaneko, J. Iwasaki, M. Kawasaki, Y. Tokura, and N. Nagaosa, Memory functions of magnetic skyrmions, *Japanese Journal of Applied Physics* **54**, 053001 (2015).
- [55] K. M. Song, J.-S. Jeong, B. Pan, X. Zhang, J. Xia, S. Cha, T.-E. Park, K. Kim, S. Finizio, J. Raabe, J. Chang, Y. Zhou, W. Zhao, W. Kang, H. Ju, and S. Woo, Skyrmion-based artificial synapses for neuromorphic computing, *Nature Electronics* **3**, 148 (2020).
- [56] W. Kang, Y. Huang, C. Zheng, W. Lv, N. Lei, Y. Zhang, X. Zhang, Y. Zhou, and W. Zhao, Voltage controlled magnetic skyrmion motion for racetrack memory, *Scientific Reports* **6**, 23164 (2016).
- [57] J. Sampaio, V. Cros, S. Rohart, A. Thiaville, and A. Fert, Nucleation, stability and current-induced motion of isolated magnetic skyrmions in nanostructures, *Nature Nanotechnology* **8**, 839 (2013).
- [58] N. Romming, C. Hanneken, M. Menzel, J. E. Bickel, B. Wolter, K. von Bergmann, A. Kubetzka, and R. Wiesendanger, Writing and deleting single magnetic skyrmions, *Science* **341**, 636 (2013).
- [59] P. Lai, G. P. Zhao, H. Tang, N. Ran, S. Q. Wu, J. Xia, X. Zhang, and Y. Zhou, An improved racetrack structure for transporting a skyrmion, *Scientific Reports* **7**, 45330 (2017).
- [60] H. T. Fook, W. L. Gan, and W. S. Lew, Gateable skyrmion transport via field-induced potential barrier modulation, *Scientific Reports* **6**, 21099 (2017).
- [61] A. A. Thiele, Steady-state motion of magnetic domains, *Phys. Rev. Lett.* **30**, 230 (1973).
- [62] K. Everschor, M. Garst, B. Binz, F. Jonietz, S. Mühlbauer, C. Pfleiderer, and A. Rosch, Rotating skyrmion lattices by spin torques and field or temperature gradients, *Phys. Rev. B* **86**, 054432 (2012).
- [63] S.-Z. Lin, C. Reichhardt, C. D. Batista, and A. Saxena, Particle model for skyrmions in metallic chiral magnets: Dynamics, pinning, and creep, *Phys. Rev. B* **87**, 214419 (2013).
- [64] A. Thiaville, Y. Nakatani, J. Miltat, and Y. Suzuki, Micromagnetic understanding of current-driven domain wall motion in patterned nanowires, *Europhysics Letters* **69**, 990 (2005).
- [65] J. Iwasaki, M. Mochizuki, and N. Nagaosa, Current-induced skyrmion dynamics in constricted geometries, *Nature Nanotechnology* **8**, 742 (2013).
- [66] J. Iwasaki, M. Mochizuki, and N. Nagaosa, Universal current-velocity relation of skyrmion motion in chiral magnets, *Nature Communications* **4**, 1463 (2013).
- [67] J. Zang, M. Mostovoy, J. H. Han, and N. Nagaosa, Dynamics of skyrmion crystals in metallic thin films, *Phys. Rev. Lett.* **107**, 136804 (2011).
- [68] W. Jiang, X. Zhang, G. Yu, W. Zhang, X. Wang, M. Benjamin Jungfleisch, J. E. Pearson, X. Cheng, O. Heinonen, K. L. Wang, Y. Zhou, A. Hoffmann, and S. G. E. te Velthuis, Direct observation of the skyrmion Hall effect, *Nature Physics* **13**, 162 (2017).
- [69] K. Litzius, I. Lemesch, B. Krüger, P. Bassirian, L. Caretta, K. Richter, F. Büttner, K. Sato, O. A. Tretiakov, J. Förster, R. M. Reeve, M. Weigand, I. Bykova, H. Stoll, G. Schütz, G. S. D. Beach, and

- M. Kläui, Skyrmion Hall effect revealed by direct time-resolved X-ray microscopy, *Nature Physics* **13**, 170 (2017).
- [70] R. Juge, S.-G. Je, D. d. S. Chaves, L. D. Buda-Prejbeanu, J. Peña Garcia, J. Nath, I. M. Miron, K. G. Rana, L. Aballe, M. Foerster, F. Genuzio, T. O. Mentès, A. Locatelli, F. Maccherozzi, S. S. Dhési, M. Belmeguenai, Y. Roussigné, S. Auffret, S. Pizzini, G. Gaudin, J. Vogel, and O. Boulle, Current-driven skyrmion dynamics and drive-dependent skyrmion Hall effect in an ultrathin film, *Phys. Rev. Appl.* **12**, 044007 (2019).
- [71] S. Woo, K. M. Song, X. Zhang, Y. Zhou, M. Ezawa, X. Liu, S. Finizio, J. Raabe, N. J. Lee, S.-I. Kim, S.-Y. Park, Y. Kim, J.-Y. Kim, D. Lee, O. Lee, J. W. Choi, B.-C. Min, H. C. Koo, and J. Chang, Current-driven dynamics and inhibition of the skyrmion Hall effect of ferrimagnetic skyrmions in GdFeCo films, *Nature Communications* **9**, 959 (2018).
- [72] C. Schütte, J. Iwasaki, A. Rosch, and N. Nagaosa, Inertia, diffusion, and dynamics of a driven skyrmion, *Phys. Rev. B* **90**, 174434 (2014).
- [73] I. Makhfudz, B. Krüger, and O. Tchernyshyov, Inertia and chiral edge modes of a skyrmion magnetic bubble, *Phys. Rev. Lett.* **109**, 217201 (2012).
- [74] X. Wu and O. Tchernyshyov, How a skyrmion can appear both massive and massless, *SciPost Phys.* **12**, 159 (2022).
- [75] S.-Z. Lin, C. D. Batista, and A. Saxena, Internal modes of a skyrmion in the ferromagnetic state of chiral magnets, *Phys. Rev. B* **89**, 024415 (2014).
- [76] M. Ezawa, Compact merons and skyrmions in thin chiral magnetic films, *Phys. Rev. B* **83**, 100408 (2011).
- [77] J. Müller, J. Rajeswari, P. Huang, Y. Murooka, H. M. Rønnow, F. Carbone, and A. Rosch, Magnetic skyrmions and skyrmion clusters in the helical phase of Cu₂OSeO₃, *Phys. Rev. Lett.* **119**, 137201 (2017).
- [78] D. Song, W. Wang, J.-X. Yu, P. Zhang, S. S. Pershoguba, G. Yin, W. Wei, J. Jiang, B. Ge, X. Fan, M. Tian, A. Rosch, J. Zang, and H. Du, Experimental observation of one-dimensional motion of interstitial skyrmion in FeGe (2022), [arXiv:2212.08991](https://arxiv.org/abs/2212.08991).
- [79] L. Kong, X. Chen, W. Wang, D. Song, and H. Du, Dynamics of interstitial skyrmions in the presence of temperature gradients, *Phys. Rev. B* **104**, 214407 (2021).
- [80] P. Schoenherr, J. Müller, L. Köhler, A. Rosch, N. Kanazawa, Y. Tokura, M. Garst, and D. Meier, Topological domain walls in helimagnets, *Nature Physics* **14**, 465 (2018).
- [81] M. Weïßenhofer, *Stochastic and Deterministic Dynamics of Topological Spin Textures : Theory and Simulation*, Ph.D. thesis, Universität Konstanz, Konstanz (2022).
- [82] D. Schick, M. Weïßenhofer, L. Rózsa, J. Rothörl, P. Virnau, and U. Nowak, Two levels of topology in skyrmion lattice dynamics, *Phys. Rev. Res.* **6**, 013097 (2024).
- [83] Y. Guang, X. Zhang, Y. Liu, L. Peng, F. S. Yasin, K. Karube, D. Nakamura, N. Nagaosa, Y. Taguchi, M. Mochizuki, Y. Tokura, and X. Yu, Confined anti-skyrmion motion driven by electric current excitations, *Nature Communications* **15**, 7701 (2024).
- [84] H. Du, R. Che, L. Kong, X. Zhao, C. Jin, C. Wang, J. Yang, W. Ning, R. Li, C. Jin, X. Chen, J. Zang, Y. Zhang, and M. Tian, Edge-mediated skyrmion chain and its collective dynamics in a confined geometry, *Nature Communications* **6**, 8504 (2015).
- [85] R. Knapman, D. R. Rodrigues, J. Masell, and K. Everschor-Sitte, Current-induced H-shaped-skyrmion creation and their dynamics in the helical phase, *Journal of Physics D: Applied Physics* **54**, 404003 (2021).
- [86] D. Song, W. Wang, S. Zhang, Y. Liu, N. Wang, F. Zheng, M. Tian, R. E. Dunin-Borkowski, J. Zang, and H. Du, Steady motion of 80-nm-size skyrmions in a 100-nm-wide track, *Nature Communications* **15**, 5614 (2024).
- [87] I. Purnama, W. L. Gan, D. W. Wong, and W. S. Lew, Guided current-induced skyrmion motion in 1D potential well, *Scientific Reports* **5**, 10620 (2015).
- [88] J. Müller, Magnetic skyrmions on a two-lane racetrack, *New Journal of Physics* **19**, 025002 (2017).
- [89] D. Liang, J. P. DeGrave, M. J. Stolt, Y. Tokura, and S. Jin, Current-driven dynamics of skyrmions stabilized in MnSi nanowires revealed by topological Hall effect, *Nature Communications* **6**, 8217 (2015).
- [90] S. Hoshino and N. Nagaosa, Theory of the magnetic skyrmion glass, *Phys. Rev. B* **97**, 024413 (2018).
- [91] C. Reichhardt, C. J. O. Reichhardt, and M. V. Milošević, Statics and dynamics of skyrmions interacting with disorder and nanostructures, *Rev. Mod. Phys.* **94**, 035005 (2022).
- [92] B. Ivanov and V. Stephanovich, Two-dimensional soliton dynamics in ferromagnets, *Physics Letters A* **141**, 89 (1989).
- [93] K.-W. Moon, B. S. Chun, W. Kim, Z. Q. Qiu, and C. Hwang, Control of skyrmion magnetic bubble gyration, *Phys. Rev. B* **89**, 064413 (2014).
- [94] M.-W. Yoo, F. Mineo, and J.-V. Kim, Analytical model of the deformation-induced inertial dynamics of a magnetic vortex, *Journal of Applied Physics* **129**, 053903 (2021).
- [95] T. Shiino, K.-J. Kim, K.-S. Lee, and B.-G. Park, Inertia-driven resonant excitation of a magnetic skyrmion, *Scientific Reports* **7**, 13993 (2017).
- [96] M. Tinkham, *Introduction to Superconductivity*, 2nd ed. (Dover Publications, 2004).
- [97] T. L. Gilbert, A phenomenological theory of damping in ferromagnetic materials, *IEEE transactions on magnetics* **40**, 3443 (2004).
- [98] J. Slonczewski, Current-driven excitation of magnetic multilayers, *Journal of Magnetism and Magnetic Materials* **159**, L1 (1996).
- [99] C. Reichhardt and C. J. O. Reichhardt, Magnus-induced dynamics of driven skyrmions on a quasi-one-dimensional periodic substrate, *Phys. Rev. B* **94**, 094413 (2016).
- [100] Y.-F. Chen, Z.-X. Li, Z.-W. Zhou, Q.-L. Xia, Y.-Z. Nie, and G.-H. Guo, Nonlinear gyrotropic motion of skyrmion in a magnetic nanodisk, *Journal of Magnetism and Magnetic Materials* **458**, 123 (2018).
- [101] S. H. Strogatz, *Nonlinear dynamics and chaos*, 2nd ed. (Westview Press, 2014).
- [102] N. Nagaosa, *Quantum Field Theory in Condensed Matter Physics* (Springer Berlin Heidelberg, Berlin, Heidelberg, 1999).
- [103] We use the following definitions of elliptic integrals $K(z) = \int_0^{\pi/2} \frac{dx}{\sqrt{1-z^2 \sin^2 x}}$ and $E(z) =$

$$\int_0^{\pi/2} dx \sqrt{1 - z^2 \sin^2 x}.$$

[104] The Lambert function $W(x)$ is defined as the solution of the equation $W(x)e^{W(x)} = 1$. We are interested in the real branch $W_{-1}(x)$, which diverges at $W_{-1}(x) \rightarrow -\infty$ at $x \rightarrow -0$.

Appendix A: Derivation of the 1D equation of motion

We aim to isolate $x(t)$ from the Thiele equation (3), which is given by

$$\mathbf{G} \times (\mathbf{u}(t) - \dot{\mathbf{r}}(t)) + \mathcal{D}(\beta \mathbf{u}(t) - \alpha \dot{\mathbf{r}}(t)) - \nabla U(\mathbf{r}(t)) = \mathbf{0}$$

For the vector components, the velocity of skyrmion

$$\mathbf{v}(t) = \dot{x}(t)\hat{\mathbf{x}} + \dot{y}(t)\hat{\mathbf{y}} \quad (\text{A1})$$

and the velocity of conduction electrons

$$\mathbf{u}(t) = u_x(t)\hat{\mathbf{x}} + u_y(t)\hat{\mathbf{y}} \quad (\text{A2})$$

Here, our model is

$$U = -\frac{1}{2}k y(t)^2 + U_{\text{dis}}(x(t)) \quad (\text{A3})$$

$$\mathbf{u}(t) = u(t)\hat{\mathbf{x}} \quad (u_y(t) = 0) \quad (\text{A4})$$

Therefore, Eq. (3) can be written as a system of ODEs

$$\mathcal{G}\dot{y} + \mathcal{D}\beta u - \mathcal{D}\alpha\dot{x} - \partial_x U_{\text{dis}} = 0 \quad (\text{A5})$$

$$\mathcal{G}u - \mathcal{G}\dot{x} - \mathcal{D}\alpha\dot{y} - ky = 0 \quad (\text{A6})$$

Differentiating both Eq. (A5) & Eq. (A6) with respect to t ,

$$\ddot{y} + \frac{\mathcal{D}\beta}{\mathcal{G}}\dot{u} - \frac{\mathcal{D}\alpha}{\mathcal{G}}\ddot{x} - \frac{\partial_x^2 U_{\text{dis}}}{\mathcal{G}}\dot{x} = 0 \quad (\text{A7})$$

$$\dot{u} - \ddot{x} - \frac{\mathcal{D}\alpha}{\mathcal{G}}\ddot{y} - \frac{k}{\mathcal{G}}\dot{y} = 0 \quad (\text{A8})$$

Eq. (A5) & Eq. (A7) can be written

$$\dot{y} = \frac{\mathcal{D}\alpha}{\mathcal{G}}\dot{x} - \frac{\mathcal{D}\beta}{\mathcal{G}}u + \frac{\partial_x U_{\text{dis}}}{\mathcal{G}} \quad (\text{A9})$$

$$\ddot{y} = \frac{\mathcal{D}\alpha}{\mathcal{G}}\ddot{x} - \frac{\mathcal{D}\beta}{\mathcal{G}}\dot{u} + \frac{\partial_x^2 U_{\text{dis}}}{\mathcal{G}}\dot{x} \quad (\text{A10})$$

Plugging in Eq. (A9) & Eq. (A10) into (A5), one can get rid of $y(t)$ and get a differential equation of $x(t)$,

$$\begin{aligned} \mathcal{G}\dot{u} - \mathcal{G}\ddot{x} - \mathcal{D}\alpha \left(\frac{\mathcal{D}\alpha}{\mathcal{G}}\dot{x} - \frac{\mathcal{D}\beta}{\mathcal{G}}\dot{u} + \frac{\partial_x^2 U_{\text{dis}}}{\mathcal{G}}\dot{x} \right) \\ - k \left(\frac{\mathcal{D}\alpha}{\mathcal{G}}\dot{x} - \frac{\mathcal{D}\beta}{\mathcal{G}}\dot{u} + \frac{\partial_x U_{\text{dis}}}{\mathcal{G}} \right) = 0 \end{aligned} \quad (\text{A11})$$

Assuming k is nonzero, we derive Eq. (8).

Appendix B: Derivation of current-velocity relation for strictly constricted 1D motion

Eq. (17) is given by

$$\frac{d\tilde{x}}{d\tilde{t}} = \tilde{u} - \sin\tilde{x}.$$

We separate \tilde{x} . We integrate over the one time period of motion \tilde{T} with respect to \tilde{t} , and integration range with respect to \tilde{x} is over the period 2π , given by

$$\tilde{T}(\tilde{u}) = \int_0^{2\pi} d\tilde{x} \frac{1}{\tilde{u} - \sin(\tilde{x})} \quad (\text{B1})$$

This can be transformed into a complex integration along a path $C : z = e^{i\tilde{x}}$ ($0 \leq \tilde{x} \leq 2\pi$),

$$\begin{aligned} \tilde{T}(\tilde{u}) &= \int_0^{2\pi} d\tilde{x} \frac{1}{\tilde{u} - \sin(\tilde{x})} \quad (\text{B2}) \\ &= \oint_C \frac{dz}{iz} \frac{1}{\tilde{u} - \frac{1}{2i}(z - \frac{1}{z})} \\ &= \oint_C dz \frac{-2}{(z - i(\sqrt{\tilde{u}^2 - 1} + \tilde{u}))(z - i(-\sqrt{\tilde{u}^2 - 1} + \tilde{u}))} \quad (\text{B3}) \end{aligned}$$

Therefore, following the residue theorem, we get

$$\tilde{T}(\tilde{u}) = \begin{cases} \infty & \text{if } 0 < \tilde{u} \leq 1 \\ \frac{2\pi}{\sqrt{\tilde{u}^2 - 1}} & \text{if } 1 \leq \tilde{u} \end{cases} \quad (\text{B4})$$

Immediately, we can get the average velocity of a skyrmion $\langle \tilde{v}_{\text{sk}} \rangle$ in terms of \tilde{u} , given by

$$\langle \tilde{v}_{\text{sk}} \rangle = \frac{2\pi}{\tilde{T}(\tilde{u})} \quad (\text{B5})$$

which leads to the relation (18).

In the following, we obtain the asymptotic form of the large current density limit and the critical current density limit in (18). In the large current density limit where $\tilde{u} \gg 1$,

$$\langle \tilde{v}_{\text{sk}} \rangle \approx \tilde{u} \quad (\text{B6})$$

so that in the dimensional form,

$$\langle v_{\text{sk}} \rangle \approx \frac{\beta}{\alpha} u \quad (\text{B7})$$

In the vicinity of the critical current density $\tilde{u}_{\text{cr}} = 1$, let $\tilde{u} = \tilde{u}_{\text{cr}} + \tilde{\epsilon}$ where $\tilde{\epsilon} \ll 1$,

$$\begin{aligned} \langle \tilde{v}_{\text{sk}} \rangle &= \sqrt{\tilde{u}^2 - 1} = \sqrt{(\tilde{u}_{\text{cr}} + \tilde{\epsilon})^2 - 1} \\ &\approx \sqrt{2\tilde{u}_{\text{cr}}\tilde{\epsilon}} = \sqrt{2\tilde{u}_{\text{cr}}}(\tilde{u} - \tilde{u}_{\text{cr}})^{1/2} \quad (\text{B8}) \end{aligned}$$